**Showcasing research from the groups of M Sc. Yuma Nakagawa and Professor Kingo Uchida at Ryukoku University, Japan and Professor Satoshi Yokojima at Tokyo University of Pharmacy and Life Sciences, Japan.**

White light emission generated by two stacking patterns of a single organic molecular crystal

White light emission based on dual emission from the crystal of single chromophore, which was produced by the oxidative photocyclization condensates of diarylethene, was reported. This crystal of single chromophore is obtained by self-assembly with distinct π–π stacking. They show structureless yellow emission due to the excited multimer in addition to blue monomer emission. Experimental and theoretical studies have shown that white light emission is based on a balanced dual emission produced by two different stacking patterns having different overlapping areas in the crystal.

ROYAL SOCIETY OF CHEMISTRY
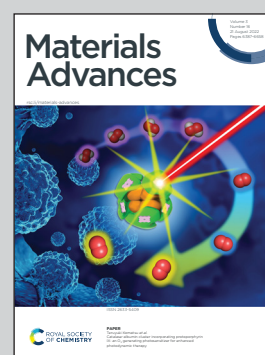
rsc.li/materials-advances

Check for updates

White light emission generated by two stacking patterns of a single organic molecular crystal†

Yuma Nakagawa, [iD] *[a] Kuon Kinoshita,[a] Megumi Kasuno,[a] Ryo Nishimura, [iD] [b]
Masakazu Morimoto, [iD] [b] Satoshi Yokojima, [iD] *[cd] Makoto Hatakeyama, [iD] [de]
Yuki Sakamoto, [iD] [d] Shinichiro Nakamura[df] and Kingo Uchida [iD] *[ad]

Dual emission by monomers and excimers is expected for single-molecule white light emitters. However, in the case of a system with an ideal excimer in a single conformation, it is very difficult to achieve their dual emission unless they have multiple chromophores in the molecule. Here, we report single-chromophore white light emission based on dual emission from the aggregation/crystallization of oxidative photocyclization condensates of diarylethene. These condensates form distinct π–π stacking by aggregation/crystallization and show structureless yellow emission due to the excited multimer in addition to blue monomer emission. Especially in the crystalline state, white light emission was observed at the International Commission on Illumination (CIE) 1931 coordinates of (0.31, 0.30). Experimental and theoretical studies have shown that white light emission is based on a balanced dual emission produced by two different stacking patterns having different overlapping areas in the crystal.

Introduction

Organic light-emitting molecules having a π-conjugated structure are used in a wide range of fields such as organic light-emitting diodes (OLEDs), chemical sensors, and fluorescent probes.[1–3] Most of these materials exhibit strong fluorescence emission in dilute solution but weak or even quenched fluorescence, termed "aggregation-caused quenching" (ACQ), in the solid state.[4] ACQ is generally produced by the formation of delocalized excitons *via* strong intermolecular π–π stacking interactions between molecules in the aggregated state. Therefore, various methods such as "aggregation-induced emission" (AIE)[4] and "crystallization-induced emission enhancement" (CIEE)[5] have been proposed to improve the fluorescence efficiency of organic light-emitting

materials in the solid state. The structural feature of molecules showing AIE and CIEE is a highly twisted configuration that avoids the possibility of intermolecular π–π interaction. As a result, intramolecular motions (intramolecular rotation and vibration) are restricted and non-radioactive decay pathways are suppressed.[4,6] Nonetheless, some planar conjugated molecules also exhibit the AIE property with excimer fluorescence from pairwise stacking states.[6] Therefore, intermolecular π–π stacking may exhibit molecular aggregation-based emission such as excimers as well as ACQ.

White organic light-emitting materials have long attracted great attention due to their fundamental importance and practical applications.[7–10] White light emission is achieved by the combination of two (blue and yellow/orange) or three emitted colours (blue, green, and red). Most examples reported so far have relied on combinations of multiple components with emission colours that cover the entire visible range.[11–13] Compared to these mixed dyes, single-molecule white light emitters (SMWLEs) are expected to exhibit superior performance without segregation or colour degradation as well as improved reproducibility.[14–17] White light emission by a single molecule requires simultaneous dual or ternary emission.[9] In the simplest case of dual emission, it can be assigned to two emission-excited states: one excited state is responsible for the blue emission, and the other contributes to the yellow/orange emission. Generally, the former is the locally excited singlet state, and the latter may be the charge transfer state,[18,19] the exciter (excited dimer) state,[15,16] the proton transfer state,[20,21] through self-assembly,[22–24] or phosphorescence from triplet excited state.[14,25,26]

[a] *Department of Materials Chemistry, Faculty of Science and Technology, Ryukoku University, Seta, Otsu, Shiga 520-2194, Japan. E-mail: uchida@rins.ryukoku.ac.jp*

[b] *Department of Chemistry and Research Center for Smart Molecules, Rikkyo University, 3-34-1 Nishi-Ikebukuro, Toshima-ku, Tokyo 171-8501, Japan*

[c] *School of Pharmacy, Tokyo University of Pharmacy and Life Sciences, 1432-1 Horinouchi, Hachioji, Tokyo 192-0392, Japan*

[d] *RIKEN, Cluster for Science, Technology and Innovation Hub, Nakamura Laboratory, 2-1 Hirosawa, Wako, Saitama 351-0198, Japan*

[e] *Faculty of Pharmaceutical Science, Sanyo-Onoda City University, 1-1-1 Daigakudori, Sanyo-Onoda, Yamaguchi 756-0884, Japan*

[f] *Priority Organization for Innovation and Excellence Laboratory for Data Science, Kumamoto University, 2-39-1, Kurokami, Chuo-ku, Kumamoto 860-8555, Japan*

† Electronic supplementary information (ESI) available: Materials and methods, supplementary figures and tables. CCDC 2076557. For ESI and crystallographic data in CIF or other electronic format see DOI: https://doi.org/10.1039/d2ma00670g

Highly planar aromatic compounds, such as pyrene, often promote the formation of exciton interactions due to efficient intermolecular π–π stacking.[27] These exciton interactions in the crystalline state are affected by the π–π stacking distance between aromatic compounds, their π–π overlap area,[28,29] and the stacking manner.[30,31] Such non-covalent interactions produce a broad, structureless, and red-shifted emission band that differs from that of monomer emission. In many cases, single crystals consist of a single stacking pattern. Therefore, they result in either monomer or exciton-interaction emission. In systems formed in this single conformation, it is very difficult to achieve dual emission: one from a single molecule and the other from non-covalent multiple molecules. Therefore, one solution to this problem may be to create a system of chromophores that have multiple stacking patterns in a crystal, each with different transition orbital properties. Conformational isomerism in each monomer, achieved by restricting covalent bonds at different dihedral angles, leads to different spatial arrangements of atoms in the molecule and multiple stacking patterns.[32–34] Due to differences in electron distribution and interactions, the conformational isomers usually exhibit very different photophysical properties, including individual emission from each conformer. Using these properties, white light emission has been achieved by mixing multiple crystal polymorphs that exhibit different emission colors,[32] doping them into a polymer matrix,[33] or applying mechanical stimuli to them.[34] These approaches required manipulation of two or three colour elements to produce white light emission. To our knowledge, there is no example of such a system being used to produce white light emission in the single-crystal state.

In this work, we report the fluorescence emission properties of **1ar** (Fig. 1a). The fluorescent molecule **1ar** shows deep-blue fluorescence in areas including the near UV region (λ_{max}: 380–390 nm) with relatively high fluorescence quantum yields in the dispersed state such as in dilute solution. Interestingly, it shows white emission in the solid state (Fig. 1b). This white emission is caused by the mixing of two emissions with different wavelengths and lifetimes, *i.e.*, blue and yellow (the latter is not observed in dilute solutions). In the crystal

state of a single molecule, there are two conformers with different stacking patterns and different overlapped areas. These generate two electronically excited singlet states (monomer and excited multimer) with different transition orbital properties *via* intermolecular orbital interactions due to π–π stacking (Fig. 1c). Moreover, the packing structures are obtained through self-assembly. Since this type of self-assembly, such as recrystallization, aggregation, and solution casting methods, can be done in a straightforward manner, it is thermodynamically stable and industrially useful in practical applications.

Results and discussion

Molecular design and synthesis

There are two types of molecular aggregation: J-type and H-type.[35,36] The H-type (parallel configuration with no slipping) generally shows a blue-shifted absorption band and ideally does not fluoresce. Therefore, to achieve dual emission in the aggregated state, aggregation of the J-type is desirable. Accordingly, in an effort to induce J-type aggregation (antiparallel configuration with slipping), we designed a structure of benzo[2,1-d:3,4-d]bisthiazole (BBT; planar structure) condensed with 3,3,4,4,5,5-hexafluorocyclopentene with high ring strain at the 5,6-position. In this structure, phenyl groups were introduced at both ends.

1ar was formed upon UV light irradiation to diarylethene **1o** in *n*-hexane in the presence of iodine (I_2) by photocyclization and dehydrogenation reactions, as in the case of typical stilbenes[37] (Fig. S1 and S2, ESI†). Stilbenes are well known to undergo photocyclization to form dihydrophenanthrenes,[38] which then revert to stilbenes in the dark in a degassed solution, while in the presence of an oxidant, dihydrophenanthrenes are irreversibly converted to phenanthrenes. Such a reaction can be used to produce condensation products that allow **1o** to be transformed into the condensed product of **1ar**. This condensation reaction has also proceeded in other solvents (*e.g.*, ethanol) and oxidants (*e.g.*, tetrabutylammonium perchlorate: TBAP). As the oxidative photocyclization proceeded, the apparent hydrogen-ion concentration in the organic solvent increased and the fluorescence intensity increased significantly (Fig. S3 and S4, ESI†). These results strongly support the observation that the oxidative photocyclization reaction was in progress and that the **1ar** produced by the reaction was fluorescent. The absorption band of **1ar** was more blue-shifted than that of **1o** because its fused ring structure cut off the conjugation length in the molecule. The purified **1ar** (λ_{max}: 335 nm and ε: 3.3×10^4 M^{-1} cm^{-1}) showed deep blue emission with a maximum fluorescence wavelength of 380 nm ($\Phi_{Flu} = 0.34$) in *n*-hexane (Fig. S5, ESI†). The ^1H NMR signals derived from **1o** and **1ar** shifted to lower fields as the reaction progressed. This is likely due to the increased concentration of H^+ in the solution as the reaction progressed and the protonation of the nitrogen atoms in the thiazole rings of **1o** and **1ar** (Fig. S4, ESI†). In the absence of the oxidant, **1ar** was not produced (Fig. S1, ESI†). The synthesis of **1ar** was confirmed by ^1H, ^{13}C, and ^{19}F NMR
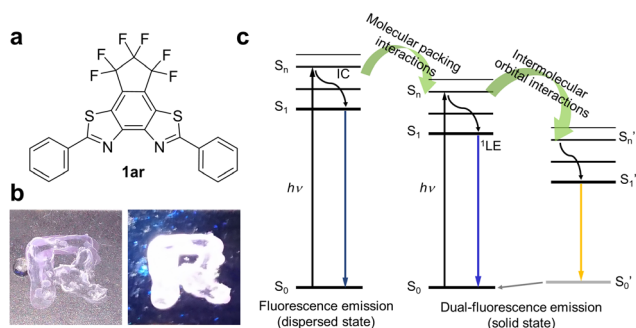

Fig. 1 (a) Molecular structure of **1ar** emitting white light in the solid state. (b) Photo-pattern of **1ar** under white light (right) and UV (λ = 365 nm, 277 mW cm^{-2}) light irradiation (left) at room temperature. The fluorescent molecule **1ar** dissolved in chloroform was drawn in an "R" pattern and dried. (c) Jablonski diagram for dual-fluorescence emission of **1ar**.

measurements, elemental analysis, and high-resolution mass spectrometry (HRMS) (see ESI† for details).

Photophysical properties

Fig. 2 shows the photophysical properties of **1ar** in the crystalline state. The absorption spectra of **1ar** crystals prepared by recrystallization from *n*-hexane are red-shifted compared to the absorption spectra in solution, suggesting a ground state interaction between the molecules (Fig. 2g). The **1ar** crystals showed white fluorescence emission when irradiated with UV light (λ = 365 nm) of the absorbance wavelength (Fig. 2a and b). There are two emission bands in **1ar** crystals: a blue emission band with a maximum fluorescence wavelength at 425 nm and a yellow emission band with a maximum fluorescence wavelength at 565 nm (Fig. 2h). In fact, when the optical filter (λ = 436 nm or λ > 500 nm) was attached to the objective lens of the digital microscope, blue and yellow fluorescence emissions were independently observed (Fig. 2c–f). Therefore, this white emission is produced by the combination of blue and yellow emissions. Fluorescence spectra are usually characterized as single emission bands that are independent of the excitation wavelength. If two emission bands are observed in the fluorescence spectrum in the solid state of a highly planar molecule, this can be attributed to one ground state having two excited state species due to excimer formation.[15,39]

The lifetime of excimer emission is often longer than that of monomer emission.[28,29,40,41] The blue fluorescence emission lifetime of **1ar** crystal was τ = 0.81 ns (Fig. 2i: blue square). In contrast, the yellow fluorescence lifetime was τ = 6.70 ns (Fig. 2i: yellow circle), which was about eight times longer than the blue fluorescence lifetime. These results strongly suggest that the yellow emission of **1ar** in the solid state is due to excimer.

Excimer is categorized into two types based on the mode of its formation.[41] One is called a "dynamic excimer", in which an excited chromophore comes into close proximity to another ground state molecule and forms an excimer. The other is called a "static excimer", in which two chromophores are conjugated by covalent or supramolecular interactions. Mainly, there are two ways to distinguish between dynamic and static excimers: analyzing excitation spectra and fluorescence lifetime decay profiles.[41–43] In the case of dynamic excimer, excitation spectra are the same when monitored at monomer- and excimer-derived emission wavelengths. Excitation spectra of **1ar** crystals at emission wavelengths at 425 and 565 nm were measured, and these spectra were very similar (Fig. S6, ESI†). In addition, the decay profile of the fluorescence lifetime at yellow (565 nm) emission showed an upward component of excimer formation characteristic of dynamic excimer followed by a negative slope of fluorescence decay (Fig. 2i). Therefore, the yellow emission of **1ar** crystal was concluded to be due to a dynamic excimer.

The International Commission on Illumination (CIE) 1931 colour space is the most well-known defined quantitative link between physically pure colours and physiologically perceived colours in human colour vision.[44] The pure white colour has CIE coordinates of (1/3, 1/3). The **1ar** crystal shows CIE coordinates of (0.31, 0.30) (Fig. 2j), which is close to the value for pure white, and its fluorescence quantum yield is 0.12. The emission quantum yields of the **1ar** crystals were in the middle range of those reported so far for molecules that emit white light in the solid state (Fig. S7 and Table S1, ESI†).

The emission properties that depend on the molecular conformation often change the emission colour upon mechanical stimulation.[32,34,45,46] The application of molecules showing such stimulation-induced phenomena to white light-emitting
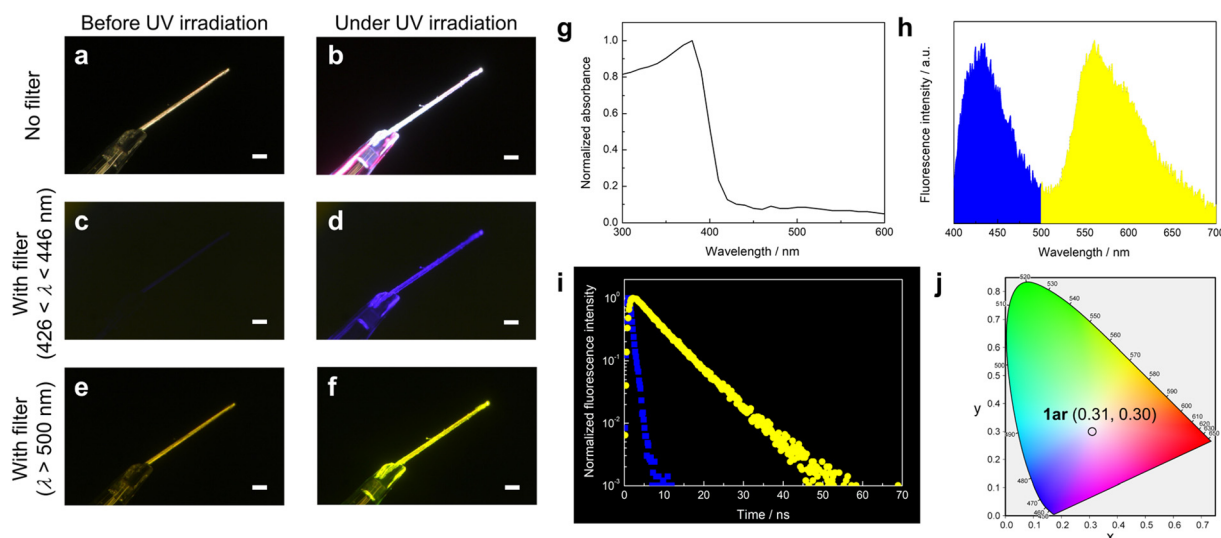

Fig. 2 (a–f) Photographs of fluorescence emission of **1ar** crystal before (a, c and e) and under UV light (λ = 365 nm, 554 mW cm^{-2}) irradiation (b, d and e). (c–f) Images taken with optical filters ((c and d): 426 < λ < 446 nm and (e and f): λ > 500 nm) attached to the objective lens of the digital microscope. Scale bars: 100 μm for (a–f). (g) Normalized absorption spectrum of **1ar** crystals. (h) Fluorescence spectrum of **1ar** crystals (λ_{exc} = 340 nm, λ_{em} = 425 and 565 nm). (i) Fluorescence decay curves of **1ar** crystals at 425 (blue square: τ = 0.81 ns) and 565 nm (yellow circle: τ = 6.70 ns) emission (λ_{exc} = 340 nm). (j) CIE 1931 coordinates of emission of **1ar** crystals (λ_{exc} = 340 nm). These observations and measurements were performed at room temperature.

devices will naturally be limited. Therefore, a promising approach would be to make molecules with no remarkable colour change even under stimulation. The powder of ground **1ar** crystals also showed white light emission due to the dual emission of blue and yellow, and its CIE coordinates were (0.35, 0.33) with a fluorescence quantum yield of 0.14 (Fig. S8, ESI†). Similarly, a film prepared by the casting method from chloroform solution also showed blue and yellow dual emission, and its CIE1931 coordinates were (0.33, 0.30) with a fluorescence quantum yield of 0.18 (Fig. S9, ESI†). In addition, no phase transition of the solid state of **1ar** was observed between melting point temperature (265 °C) and room temperature (Fig. S10, ESI†). Therefore, the molecular packing and white light emission of **1ar** is likely to be maintained at temperatures below the melting point. In fact, white light emission was observed when **1ar** in solid state was irradiated with ultraviolet light under heating at about 200 °C (Fig. S11, ESI†).

First, we investigated the polarity effect on the dual emission of **1ar** by comparing the emissions in nine different solvents. The solubility of **1ar** in organic solvents was not so good, and it was difficult to make highly concentrated solutions. Therefore, the effect of solvent polarity on the absorption and emission properties of **1ar** was performed in dilute solution. The maximum absorption and fluorescence wavelengths of **1ar** showed maximum deviations of 8 and 9 nm, respectively, and were nearly unchanged among the nine solvents (Fig. S12 and Table S2, ESI†). Then, the difference between the maximum absorption and fluorescence wavelengths ($\lambda_{em}^{max} - \lambda_{abs}^{max} = \Delta\lambda$) in these solvents was plotted against the $E_T(30)$[47] value, which is a measure of solvent polarity. The results show that **1ar** has a relatively small positive correlation with $E_T(30)$. The fluorescence quantum yield of **1ar** was also measured in the nine different kinds of solvents, with resulting values in the range of 0.3–0.5. These results show that the optical properties such as λ_{abs}^{max}, λ_{em}^{max}, and Φ_{Flu} of **1ar** have relatively small dependence on the solvent, which excludes the polarity effect on the emission of **1ar**.

Then, to investigate the origin of the excimer emission of **1ar**, absorption and fluorescence spectra were measured at different concentrations (5–100 μM) (Fig. S13, ESI†). Absorbance increased with increasing concentration of **1ar**. Fluorescence intensity increased with increasing concentration from 5–20 μM of **1ar**, but fluorescence intensity decreased with increasing concentration above 25 μM due to concentration quenching. The normalized fluorescence spectra and these difference spectra showed red-shifted monomer emission due to intermolecular interactions, but excimer emission was not observed. Free rotation of the phenyl group at the end of **1ar** can occur in solution, which potentially creates the intermolecular distance for suppressing the excimer emission. Since **1ar** has high molecular planarity, it could form intermolecular interactions such as π–π stacking upon aggregation/crystallization. Thus, we investigated the fluorescence emission characteristics of **1ar** in its aggregated state. This state was recorded in ethanol/water mixtures containing different amounts of water, which acted as a poor solvent (Fig. 3). The maximum fluorescence at **1ar** was not significantly changed by the addition of a small amount of water (<70 vol%)
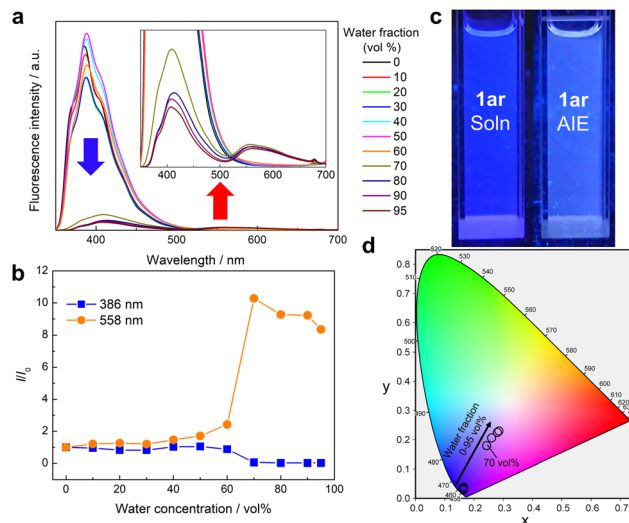

Fig. 3 (a) Fluorescence spectra of **1ar** in ethanol/water mixtures with different water contents (0–95 vol%) (**1ar**: 5 μM, λ_{exc} = 336 nm). When more than 70 vol% water was added, a new fluorescence with a maximum wavelength at 558 nm was observed in addition to the decrease in deep-blue fluorescence intensity. (b) Plots of relative fluorescence intensity (I/I_0) vs. water concentration of **1ar** at 386 or 558 nm, where I_0 is the fluorescence intensity of the ethanol solutions. (c) Photographs of fluorescence emission of **1ar** in ethanol (left) and ethanol/water = 7 : 3 (v/v) (right) under UV light (λ = 365 nm, 810 μW cm^{-2}) irradiation. (d) CIE 1931 coordinates of emission of **1ar** in different water contents (λ_{exc} = 336 nm). These observations and measurements were performed at room temperature.

(Fig. 3a and b). When more than 70 vol% water was added, a new fluorescence with a maximum wavelength at 558 nm (yellow emission region) was observed in addition to the previous decrease in deep-blue fluorescence intensity (Fig. 3a and b). The calculated CIE coordinate of **1ar** in ethanol/water mixtures approaches a white value due to the decrease in the ratio of blue to yellow emission bands as the water fraction in the solution increases (Fig. 3c and d).

Crystal structure

To clarify the white-light-emitting mechanism of **1ar** crystal, X-ray crystallographic analysis was carried out. A rod-shaped single crystal of **1ar**, suitable for X-ray crystallographic analysis, was prepared by recrystallization from *n*-hexane. The details of the crystal structure of **1ar** are shown in Fig. S14 and Table S3 (ESI†). In the crystal, there are two crystallographically independent conformers with similar bond lengths and dihedral angles (Fig. 4 and Table S4, ESI†). They are arranged in an alternating zigzag pattern, indicating herringbone packing. Each conformer is antiparallel to the same conformer with slipping, and each of those conformers forms a column with a ladder arrangement. There are two types of stacking dimers for each conformer. These dimers are referred to Type 1 and 2 dimers for conformer A and Type 3 and Type 4 dimers for conformer B (Fig. 4b). The interplanar distances between two blue (bright yellow) conformers, which correspond to Type 1 and Type 2 (Type 3 and Type 4) dimers, are 3.414 and 3.493
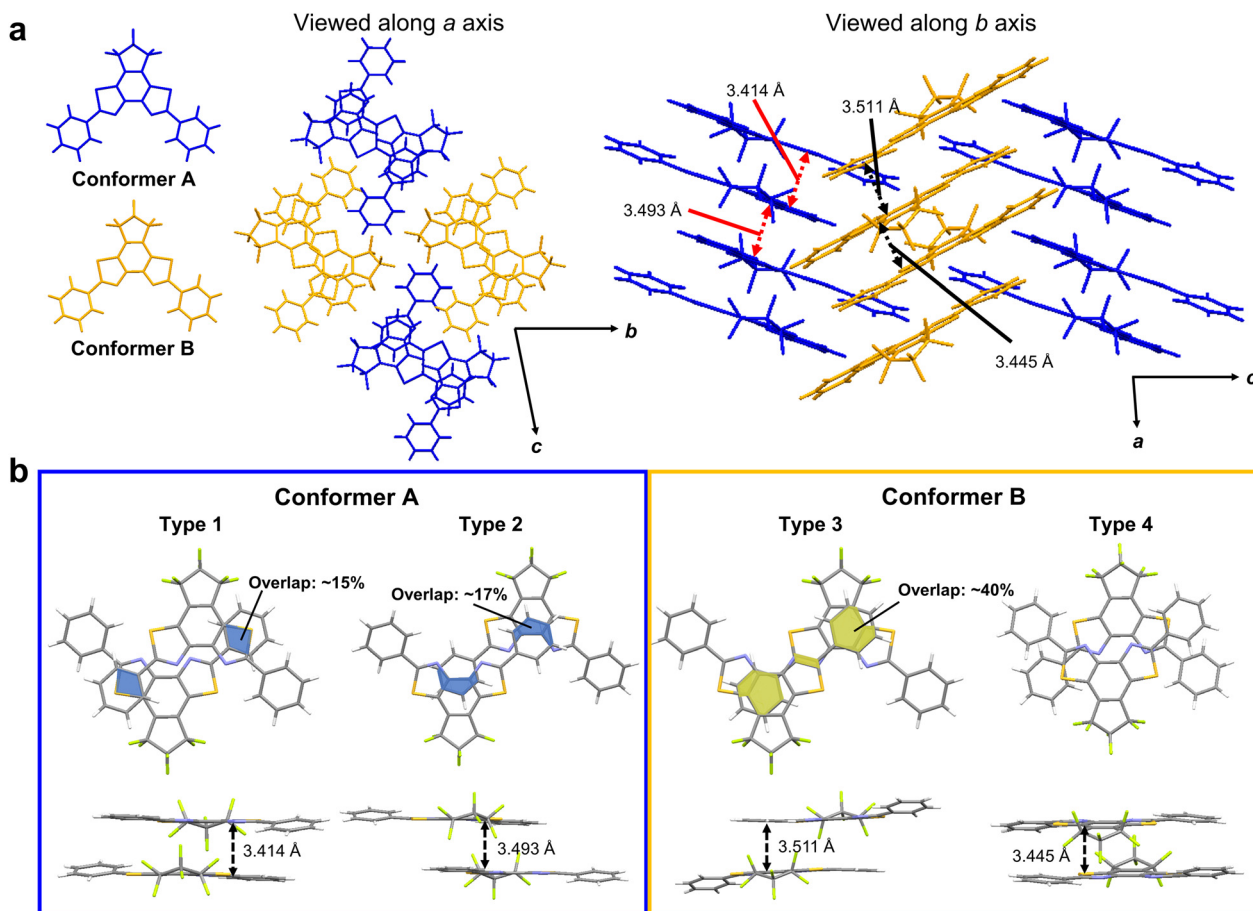
Fig. 4 (a) Packing mode in **1ar** crystal obtained by recrystallization from hexane solution. In the crystal, there are two independent conformers (blue and bright yellow). (b) Summary of interplanar distances and overlap regions for each of the conformers of **1ar** in the crystal. The overlap ratio is calculated based on BBT.

(3.493 and 3.445), respectively. These interplanar distances are typical for π–π stacking molecules,[48] and they strongly suggest the existence of π–π interactions.

To examine the effect of these structures to the characteristics of excited states, we performed quantum chemical calculations for monomers, stacked dimers, a unit cell, two adjacent unit cells, and 8mer or 9mer as specified in Supporting Information. In our calculations, we found that the excited states spread over many molecules as the cluster size increases, that is, a redshift of the wavelength of the lowest absorption edge from 349 nm to 399 nm, even for the limited size of the **1ar** cluster (9mer). Considering the further redshift with larger size together with the structural relaxation after excitation, we can assume that the fluorescence of yellow colour is due to the excited state from the many molecules. We further found that the lowest excited state has a large oscillator strength by consistently including the effect of double excitation. Thus, the computational results indicate that fluorescence occurs not only from the monomer but also from the excited state formed by multiple molecules, possibly due to the presence of multimer (for details, see Fig. S15–S20 and Tables S5–S14, ESI†).

The recent pioneering works have shown that not only the distance between the planes but also the overlap between the planes is important for π–π interaction.[28,29] A π–π overlap of more than 40% could potentially cause a red-shift in emission wavelength by more than 100 nm.[29] This advantageous overlap has the potential to induce excimer emission.[28] In the case of conformer A, there was an overlap between the phenyl group and the BBT unit, but the overlap regions were very narrow, at less than 20%. In conformer B, there was more than twice as much overlap as in conformer A. Moreover, there is a very narrow but overlapping region between the BBT units. Therefore, the dimer of conformer B with its usefully wide overlap region is expected to provide excimer emission.

We thus attribute the blue emission to the superposition of the monomer excitation over multiple molecules of the conformer A and the yellow emission to the excimer on the conformer B.

Control of emission properties of polymer composite film

Deep-blue light emission (emission peak $\lambda < 450$ nm) as well as white light emission is very important. Deep-blue light emitting materials have great potential to function as light-converting materials as well as fluorescence-based chemical and biological sensors.[49,50] However, the solid state of **1ar** shows white light emission instead of deep-blue light emission due to the
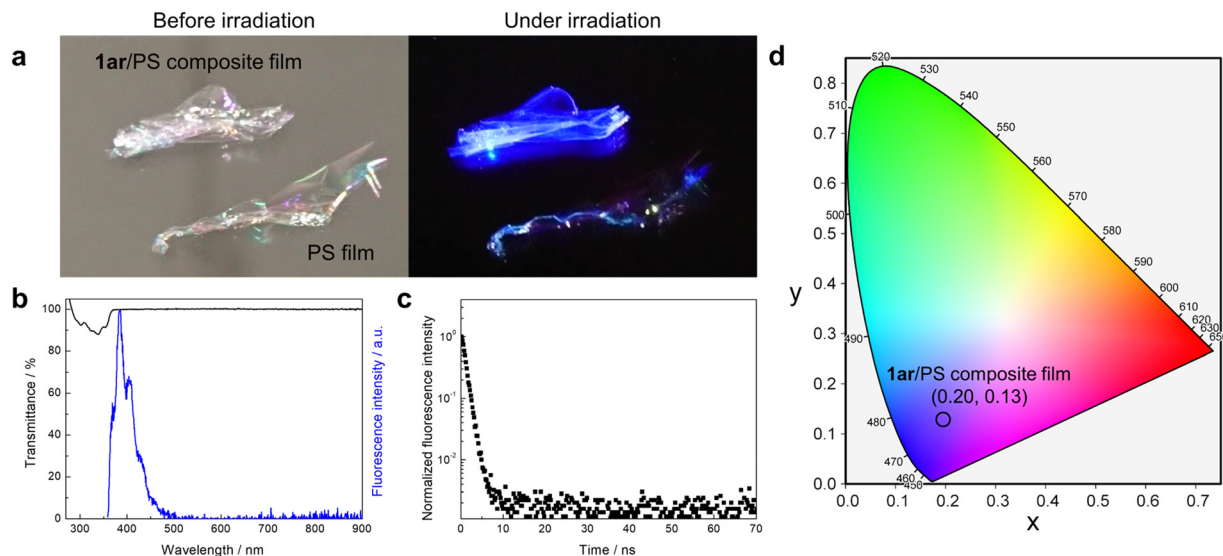
Fig. 5 (a) Photographs of **1ar**/PS composite film (ratio of **1ar**: 0.01 wt%) and PS film before (left) and under UV light (λ = 365 nm) irradiation (right). (b) Transmittance (black line) and fluorescence (blue line) spectra of **1ar**/PS composite film (λ_{exc} = 336 nm, λ_{em} = 382 nm). (c) Fluorescence decay curve of **1ar**/PS composite film (λ_{exc} = 340 nm, λ_{em} = 382 nm, τ = 1.00 ns). (d) CIE 1931 coordinates of emission of **1ar**/PS composite film (λ_{exc} = 336 nm). These observations and measurements were performed at room temperature.

formation of intermolecular interactions by aggregation. Dispersion of **1ar** in the polymer matrix is an effective strategy to avoid this. Here, solid films were prepared by dispersing **1ar** in polystyrene (PS). The produced film is very transparent (about 100% transmittance in the entire visible region: Fig. 5a and b) under daylight conditions. Under UV light irradiation, it then shows deep-blue fluorescence emission (Fig. 5a and b). The fluorescence spectra and fluorescence quantum yield (Φ_{Flu} = 0.34) of the prepared **1ar**/PS composite film were almost the same as those of the *n*-hexane solution, and the fluorescence lifetime was almost the same as that of the blue emission band of **1ar** in the crystalline state (Fig. 5c).

To further investigate the formation of excimer, **1ar**/PS composite films with increasing concentrations of **1ar** were prepared (Fig. S21, ESI†). As the concentration of **1ar** in the **1ar**/PS composite film increased, a structureless yellow emission at 565 nm appeared at 20 wt% or more. In addition, the fluorescence lifetime of the blue and yellow emissions of these films was similar to that of **1ar** crystal, and the emission colour approaches white light as the concentration of **1ar** increases. The observation of such concentration-dependent emission can be attributed to excimer emission caused by the molecules packing more tightly together at higher concentrations, as in the **1ar** crystal.

Conclusions

In summary, white light emission based on dual emission of oxidative photocyclization condensates of diarylethene in the solid state was reported. In dilute solutions and in PS composite films with concentrations of 10 wt% or less, the condensation product shows deep blue emission due to the absence of intermolecular orbital interactions, but in the aggregated state,

it shows structureless yellow emission due to the formation of intermolecular orbital interactions in addition to the monomer-derived blue emission. Here, **1ar** is SMWLE, which in the crystalline state shows white emission at CIE1931 coordinates of (0.31, 0.30). Our experimental and theoretical investigations show that white light emission is based on a balanced dual emission produced by two conformers with different stacking patterns and overlapping areas in the crystal. Interestingly, the packing structure with these two conformers, which results in white light emission, is achieved by self-assembly. Therefore, white light emission of **1ar** was observed in all of the crystal, powder, and cast film. White light is used in a variety of applications, including the backlight of display, lighting, and illumination. Although inorganic materials still account for a majority of these devices, some works are starting to use organic materials. The white light emission achieved by self-assembly of **1ar** has the potential to provide excellent processability in the fabrication of these devices. Thus, we believe our current results will provide important clues for the development of organic materials for applications in the future.

Author contributions

Y. Nakagawa and K. Kinoshita synthesized all materials. Y. Nakagawa grew the crystals, performed all photophysical measurements and analyses, and prepared the paper. R. Nishimura and M. Morimoto performed the X-ray crystallographic analysis. Y. Nakagawa, S. Yokojima, M. Hatakeyama, and Y. Sakamoto performed the theoretical calculations. S. Yokojima and S. Nakamura supervised the theoretical calculations. M. Kasuno assisted the pH measurement. K. Uchida supervised the research. So, S. Yokojima, S. Nakamura, and K. Uchida

jointly supervised this work. All authors discussed the results and commented on the manuscript.

Conflicts of interest

There are no conflicts to declare.

Acknowledgements

Notes and references

1 J. H. Burroughes, D. D. C. Bradley, A. R. Brown, R. N. Marks, K. Mackay, R. H. Friend, P. L. Burns and A. B. Holmes, *Nature*, 1990, **347**, 539–541.
2 O. Ostroverkhova, *Chem. Rev.*, 2016, **116**, 13279–13412.
3 Y. Yang, Q. Zhao, W. Feng and F. Li, *Chem. Rev.*, 2013, **113**, 192–270.
4 Y. Hong, J. W. Y. Lam and B. Z. Tang, *Chem. Soc. Rev.*, 2011, **40**, 5361–5388.
5 J. Tong, Y. J. Wang, Z. Wang, J. Z. Sun and B. Z. Tang, *J. Phys. Chem. C*, 2015, **119**, 21875–21881.
6 Q. Li and Z. Li, *Adv. Sci.*, 2017, **4**, 1600484.
7 Y. Yin, M. U. Ali, W. Xie, H. Yang and H. Meng, *Mater. Chem. Front.*, 2019, **3**, 970–1031.
8 S. Mukherjee and P. Thilagar, *Dyes Pigm.*, 2014, **110**, 2–27.
9 G. M. Farinola and R. Ragni, *Chem. Soc. Rev.*, 2011, **40**, 3467–3482.
10 K. T. Kamtekar, A. P. Monkman and M. R. Bryce, *Adv. Mater.*, 2010, **22**, 572–582.
11 R. W. Pridmore, *Color Res. Appl.*, 2009, **34**, 233–252.
12 L. Simonot and M. Hébert, *J. Opt. Soc. Am. A*, 2014, **31**, 58–66.
13 V. K. Vishwakarma, M. R. Nagar, N. Lhouvum, J. H. Jou and A. A. Sudhakar, *Adv. Opt. Mater.*, 2022, **10**, 2200241.
14 Z. He, W. Zhao, J. W. Y. Lam, Q. Peng, H. Ma, G. Liang, Z. Shuai and B. Z. Tang, *Nat. Commun.*, 2017, **8**, 416.
15 Q. Y. Yang and J. M. Lehn, *Angew. Chem., Int. Ed.*, 2014, **53**, 4572–4577.
16 Y. H. Chen, K. C. Tang, Y. T. Chen, J. Y. Shen, Y. S. Wu, S. H. Liu, C. S. Lee, C. H. Chen, T. Y. Lai, S. H. Tung, R. J. Jeng, W. Y. Hung, M. Jiao, C. C. Wu and P. T. Chou, *Chem. Sci.*, 2016, **7**, 3556–3563.
17 Z. Xie, C. Chen, S. Xu, J. Li, Y. Zhang, S. Liu, J. Xu and Z. Chi, *Angew. Chem., Int. Ed.*, 2015, **54**, 7181–7184.
18 Z. R. Grabowski, K. Rotkiewicz and W. Rettig, *Chem. Rev.*, 2003, **103**, 3899–4032.
19 X. H. Jin, C. Chen, C. X. Ren, L. X. Cai and J. Zhang, *Chem. Commun.*, 2014, **50**, 15878–15881.
20 Y. Yang, M. Lowry, C. M. Schowalter, S. O. Fakayode, J. O. Escobedo, X. Xu, H. Zhang, T. J. Jensen, F. R. Fronczek, I. M. Warner and R. M. Strongin, *J. Am. Chem. Soc.*, 2006, **129**, 14081–14092.
21 D. Li, W. Hu, J. Wang, Q. Zhang, X. M. Cao, X. Ma and H. Tian, *Chem. Sci.*, 2018, **9**, 5709–5715.
22 S. Samanta, U. Manna and G. Das, *New J. Chem.*, 2017, **41**, 1064–1072.
23 K. Pal, V. Sharma and A. L. Koner, *Chem. Commun.*, 2017, **53**, 7909–7912.
24 N. Kapuria, V. Sharma, P. Kumar and A. L. Koner, *J. Mater. Chem. C*, 2018, **6**, 11328–11335.
25 Y. Wang, Q. Sun, L. Yue, J. Ma, S. Yuan, D. Liu, H. Zhang, S. Xue and W. Yang, *Adv. Opt. Mater.*, 2021, **9**, 2101075.
26 J. Ma, Y. Zhou, H. Gao, F. Zhu and G. Liang, *Mater. Chem. Front.*, 2021, **5**, 2261–2270.
27 S. Kundu, B. Sk, P. Pallavi, A. Giri and A. Patra, *Chem. – Eur. J.*, 2020, **26**, 5557–5582.
28 Y. Ge, Y. Wen, H. Liu, T. Lu, Y. Yu, X. Zhang, B. Li, S. T. Zhang, W. Li and B. Yang, *J. Mater. Chem. C*, 2020, **8**, 11830–11838.
29 T. Schillmöller, R. Herbst-Irmer and D. Stalke, *Adv. Opt. Mater.*, 2021, **9**, 2001814.
30 B. Shi, D. Nachtigallová, A. J. A. Aquino, F. B. C. Machado and H. Lischka, *Phys. Chem. Chem. Phys.*, 2019, **21**, 9077–9088.
31 A. Sakai, E. Ohta, Y. Yoshimoto, M. Tanaka, Y. Matsui, K. Mizuno and H. Ikeda, *Chem. – Eur. J.*, 2015, **21**, 18128–18137.
32 Y. Zhang, Y. Miao, X. Song, Y. Gao, Z. Zhang, K. Ye and Y. Wang, *J. Phys. Chem. Lett.*, 2017, **8**, 4808–4813.
33 B. Li, Z. Li, F. Guo, J. Song, X. Jiang, Y. Wang, S. Gao, J. Wang, X. Pang, L. Zhao and Y. Zhang, *ACS Appl. Mater. Interfaces*, 2020, **12**, 14233–14243.
34 Z. He, X. Cai, Z. Wang, D. Chen, Y. Li, H. Zhao, K. Liu, Y. Cao and S. J. Su, *Sci. China: Chem.*, 2018, **61**, 677–686.
35 N. J. Hestand and F. C. Spano, *Chem. Rev.*, 2018, **118**, 7069–7163.
36 F. Würthner, T. E. Kaiser and C. R. Saha-Möller, *Angew. Chem., Int. Ed.*, 2011, **50**, 3376–3410.
37 D. H. Waldeck, *Chem. Rev.*, 1991, **91**, 415–436.
38 M. Irie, *Chem. Rev.*, 2000, **100**, 1685–1716.
39 Rohini, M. Baral and B. K. Kanungo, *RSC Adv.*, 2016, **6**, 108017–108027.
40 M. J. Snare, P. J. Thistlethwaite and K. P. Ghiggino, *J. Am. Chem. Soc.*, 1983, **105**, 3328–3332.
41 V. Kumar, B. Sk, S. Kundu and A. Patra, *J. Mater. Chem. C*, 2018, **6**, 12086–12094.
42 F. M. Winnik, *Chem. Rev.*, 1993, **93**, 587–614.
43 S. Karuppannan and J. C. Chambron, *Chem. – Asian J.*, 2011, **6**, 964–984.

44 T. Smith and J. Guild, *Trans. Opt. Soc.*, 1931, **33**, 73.

45 C. Wang and Z. Li, *Mater. Chem. Front.*, 2017, **1**, 2174–2194.

46 J. Yang, J. Qin, P. Geng, J. Wang, M. Fang and Z. Li, *Angew. Chem.*, 2018, **130**, 14370–14374.

47 C. Reichardt, *Chem. Rev.*, 1994, **94**, 2319–2358.

48 Y. Zhao, Y. Guo and Y. Liu, *Adv. Mater.*, 2013, **25**, 5372–5391.

49 P. Han, Z. Xu, C. Lin, D. Ma, A. Qin and B. Z. Tang, *J. Mater. Chem. C*, 2020, **8**, 7012–7018.

50 Z. Shen, X. Zhu, W. Tang, X. J. Feng, Z. Zhao and H. Lu, *J. Mater. Chem. C*, 2020, **8**, 9401–9409.